Efficacy of calcination on the optical, structural and photocatalytic properties of Zirconium Oxide via facile precipitation method

Dr. S. Akilandeswari[1*] G. Rajesh [2], Dr. D. Govindarajan[2]
[1*]Department of Physics, Government College for Women (Autonomous), Kumbakonam, Tamilnadu -612001, India
[2]Department of Physics, Annamalai University, Annamalai Nagar, Chidambaram, Tamilnadu- 608 002, India

Abstract: In this present work, ZrO_2 NPs were fabricated by a chemical precipitation process under different calcined at 400, 500, 600, 700 and 800ºC respectively. The prepared ZrO_2 samples were characterized for their thermal, structural, photocatalytic, morphological, chemical compositions photoluminescence and optical properties. The thermogravimetric and differential thermal analysis (TG-DTA) results showed evidence of ZrO_2 crystalline formation below 400ºC. X-ray diffraction profiles revealed ZrO_2 tetragonal structural planes without significant changes up to 800ºC. UV-DRS studies suggested that ZrO_2 nanoparticles demonstrated blue shift with a reduction in both absorption edges and energy band gap (Eg). From the spectrum strong peak 337 nm due to near band edge emissions. The optimum level of ZrO_2 NPs (600ºC) was subjected to further characterization by Field emission scanning electron microscopy (FESEM), and Fourier transform infrared spectroscopy (FT-IR). The Photocatalytic behavior of t-ZrO_2 nanoparticles (600ºC) was analyzed against hazardous Methyl violet and Methyl blue dyes.

Keywords: **Zirconium Oxide, Methyl violet, Methyl blue, Photocatalytic application.**

1. INTRODUCTION

In recent year, a rapid expansion of the textile, painting, cosmetic and leather industry has led to the ingathering of diverse organic pollutants. The expulsion of organic effluents into an arouses most important problem in our ecosystem. Various dye effluents are complicated to remove Notable conventional physiochemical techniques often employed to mitigate the detrimental impact of these pollutants includes activated carbon adsorption, chemical agents' coagulation, resins adsorbent, ultrafiltration, reverse osmosis, the oxidation process and catalytic activity [1-4].

Amongst these methods, catalytic activity is one potential approach to keep aquatic environment under clean control because of its ability to oxidize some organic pollutants. In the past, many oxide and sulfide materials have been applied for photocatalytic degradation [1][5-8]. Some of these oxides and sulfide include TiO_2, WO_3, ZnO, HfO_2, $SrTiO_3$, Al_2O_3, TiO_2, CeO_2, SnO_2, ZrO_2, Y_2O_3, ZnS, and CdS. ZrO_2 is important material worn for the deformation, isomerization, and dehydrogenation of various organic pollutants. Zirconium is an N-type semiconductor material with the large band gap of 5.0 eV. It is regarded to be an excellent oxide material for widespread applications in numerous fields, attributable to its high thermal expansion, well mechanical strength, less thermal conductivity, good thermal stability, high thermal shock resistance, good transparency and good fracture toughness [9-12]. Thus, zirconium oxide has been studied for lots of applications including: oxygen sensors [13, 14], biological material [15,16], automobile parts [10, 17], fuel cells [18, 19], thermal barrier [20, 21] and photocatalytic properties [22, 23]. Zirconium oxide mainly exhibits three crystallographic structures: namely (m-ZrO_2), tetragonal (t-ZrO_2) and cubic (c-ZrO_2). The monoclinic phase exists from room temperature up to 1175 °C. Above 1175 °C but below 2370 °C, ZrO_2 occur in its tetragonal form whereas above 2370 °C the cubic phase is dominating up to 2750 °C ranges [24, 25]. Thus, the phases are strongly depended on synthesis method and thermal condition [25]. There are a lot of methods adopted to prepare ZrO_2 nanoparticles. Some of these methods include: sol−gel processing [26], microwave irradiation [27], hydrothermal synthesis [28], spray pyrolysis [29], auto combustion [30], precipitation [31], solid-state reaction [32] and combustion [33]. In these works, we have adopted precipitation method because this method is capable of producing ultrafine (NPs) powders with eminent purity and high homogeneous powder at lesser temperatures. It is a low cost and speedy method of synthesizing ZrO_2. Zirconium oxide (ZrO_2) can only be stimulated for UV light irradiation, limits of application in visible-light [35]. Hui Wang et.al [35] detailed by pure t-ZrO_2 phase, particle sizes were controlled between 3.6–6.0 nm ranges, its mainly adopted preparation conditions. Botta SG et.al [36] reported energy gap of ZrO_2 range from 3.25 to 5.1 eV, it is mainly depending on thermal conditions and preparation techniques. Zheng et al. [37] Photocatalytic activity was done by RhB dye under ultraviolet radiation. ZrO_2 nanostructure with particle size 8nm was induced by oxygen vacancies. The aim of the current work, we have attempted ZrO_2 NPs at different calcination condition, it's induced various thermal, structural, morphological, vibrational, electrical, and optical, photocatalytic properties investigated systematically. Thus, calcination temperatures could affect ZrO_2 nanostructures crystalline phases, size,

shape as well as morphologies. These changes may be responsible for various structural, morphological, vibrational and optical properties modification. In this paper, ZrO_2 products have been successfully synthesized by a precipitation process. The harvested nanoparticles were heat treated at different calcination temperatures ranging from 400,500,600,700 to 800 °C. The ultimate products were then investigated for their structural, optical, vibrational, and morphological properties. In addition, ZrO_2 nanoparticles photocatalytic degradation of MV (Methyl violet) and MB (Methyl blue) dye was tested under ultraviolet (UV) radiation.

2. Materials and Methods

2.1. Materials

Zirconyl chloride octahydrate ($ZrOCl_2.8H_2O$), Sodium hydroxide (NaOH), Ethanol (C_2H_6O), Methyl violet (C_{25} H_{30} CIN_3), Methyl blue (C_{37} H_{27} N_3O_9 S_3 Na_2) and Acetone (C_3H_6O), were purchased from Merck and SRL Pvt. Ltd (AR grade with 99% purity) and applied without any additional purification. De-ionized water is used for sample preparation and all dilutions.

2.2. Synthesis of ZrO_2 nanoparticles:

In the study, ZrO_2 have been synthesized by the precipitation method, taking Zirconium Oxychloride octahydrate ($ZrOCl_2.8H_2O$), sodium hydroxide (NaOH) as starting materials. An appropriate quantity of Zirconium Oxychloride octahydrate ($ZrOCl_2.8H_2O$) was dissolved in de-ionized water to form a lucid solution and the aqueous solution was magnetically stirred for 30m. Afterward, NaOH solution was added into the over solution was transferred drop wise mixed well with followed by constant stirring using magnetic stirrer, while adding NaOH (sodium hydroxide), initially white color solution was formed eventually resulting in a white precipitate until the pH value is reached to 10–12. The whole mixed solution is kept on 80°C under continuously stirring to allow for 5h the final solution is formed like gel nature. The obtained white dispersion was purified by dialysis against deionized water and ethanol washed thoroughly to eliminate unwanted traces of ions. Thereafter, the solution gel was dried in hot air oven at 100°C for 6h to evaporate organic materials and water maximum extent. Finally, they obtained product $Zr(OH)_4$ was annealed at 400, 500, 600, 700 and 800 °C in a muffle furnace for 5 h. After the annealed white powders ZrO_2 were milled to finer powders utilizing agate mortar and pestle for further different characterization techniques.

$$ZrOCl_2.8H_2O + 4NaOH \rightarrow Zr(OH)_4 + 4NaCl + 7H_2O \quad (1)$$

$$Zr(OH)_4 \rightarrow ZrO_2 + 2H_2O \quad (2)$$

The $ZrOCl_2.8H_2O$ to transformed ZrO_2 involves intermediate stages and directly, does not form in single step (the equation is given 1& 2). In the beginning, coordinated terminal hydroxyl groups and water were lost. In the next step, were detected by oxolation of -OH functional group and then finally to form nuclei grow gives observable crystallite [31].

2.3. Instrumentations

Synthesized ZrO_2 powders were recorded by X-ray diffraction pattern using X'PERT PRO diffractometer, operating condition at 40 KV and 30 mA with radiation (Cu Kα = 1.54060 Å) over the scan range 10° to 70° (2θ) with a continuous scan speed of 10° m^{-1}. FT-IR was employed to characterize the functional groups and chemical composition of the synthesized sample using FT- IR spectrometer instruments (PerkinElmer) and using KBr pellet measurement range from 400 to 4000 cm^{-1}. The as-synthesized samples have been studied by TG/DTA using Perkin Elmer Diamond (NETZSCH STA 449F3) instrument at a heating rate of 20°C/ min in air. The morphology and chemical composition of ZrO_2 powders were obtained by FESEM- field emission scanning electron microscope (ZEISS Supra 40VP) with an operating voltage of 20 kV accelerating potential. EDS-Energy-dispersive spectrum (ZEISS Supra 40VP) was attached with FESEM spectrum. The optical band gap energy was measured in the wavelength range of 200- 800 nm using SHIMADZU UV 2600 (UV-Vis NIR spectrometer) with an integrating sphere and the baseline correction was performed using a calibrated reference sample of barium sulfate ($BaSO_4$).

2.4. Photocatalytic activity

The photocatalytic efficiency of the ZrO_2 (600° C) nanoparticles was evaluated by the photodegradation of Methyl violet (MV) and Methyl blue (MB) aqueous solution under UV light irradiation. Before irradiation, 0.03 g of prepared catalyst was mixed in 50 mL of (MV and MB) aqueous solution. The suspension was equilibrated by using a magnetic stirrer in a dark room for 30 min to stabilize the adsorption of the aqueous solution over the surface of the ZrO_2. After the dark room adsorption, the initial sample was collected. Irradiation process was constantly supplied with open air condition. At regular time intervals (for every 10 min), 5 mL quantity of the solution was taken and then centrifuged to separate the suspended catalyst. The concentration of the MV and MB aqueous solution in each and every sample was examined by using a UV- Vis spectrometer (SHIMADZU-UV 1800 spectrometer). The weak and strong absorption was assessed at 291 and 663 nm, 312 and 624 nm for MV and MB aqueous dyes respectively.

The dyes degradation percentage was expressed using the formula.

The degradation rate of MV and MB: $= \frac{C_0 - C_t}{C_0} \times 100\%$ (3)

Where C_0 is the initial dyes (MV and MB) concentration, C_t is the dyes (MV and MB) concentration at a certain irradiation time (t).

3. Results and Discussion

3.1. Thermo gravimetric–differential thermal analysis (TG–DTA) study

Figure.1 shows TG -DTA curves indicated thermal behaviors of as synthesized products. As-synthesized zirconium powder were attempted in the (30 to 800 °C) range of temperature with the rate of heating at 20 °C/min. The consequential as-synthesized samples showed a single weight loss given by curves (TG -27.8 wt %) at temperature ranges 32ºC to below 382°C, which is corresponding to DTA curve exhibited an endothermic at 132ºC and exothermic at 252ºC, respectively [24][35][38]. However, further increased temperature TG-DTA curves does not raise any additional characteristics. In such cases, exothermic peak represents desorption of H_2O, CO_2, and some other organic solvents are physically absorbed. It is related to the endothermic peaks to rely on the decomposition of some remainder organic moieties coming from acetylacetonate and alkoxide groups and loss of oxygen at a higher temperature, which indicates all compounds in the precursors. $Zr(OH)_4$ are decomposed completely below 400 ºC with simultaneous above 400 ºC in DTA curve there was no exothermic peak, the resulted crystallization conversion as–prepared sample, indicating an improvement of Zirconium Oxide as the ultimate product [24][38][39].

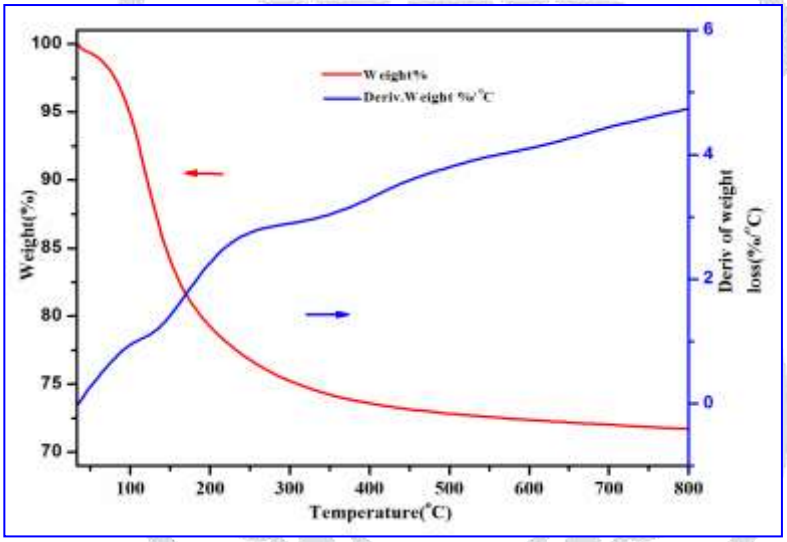

Figure 1. TG-DTA curves of the precursor of nanosized $Zr(OH)_4$

3.2. XRD analysis

The structures, purity, and crystallinity of the ZrO_2 powders were analyzed by powder X-ray diffraction measurements. Fig.2 shows the XRD patterns of synthesized samples calcined at a different temperature. From the Fig.2. it can be seen clearly, broad and large, intense peaks indicate particle size is very small crystalline nature. All the diffraction features of the synthesized samples calcined at 400, 500, 600, 700 and 800 ºC are assigned to t-ZrO_2 phase gives without any other impurities (or) signals from the phases. In addition, XRD results point out the peaks intensity gradually increased with increasing calcined temperature, signifying the increase in crystallite size (2.6,2.0,2.9,3.8,10.2 nm) owing to calcined process. These observations noted in table.1. The diffractive peaks with 2θ values of around 30, 35, 50, and 60º corresponding with, orientations to the (101), (110), (112), and (211) crystalline planes, respectively (JCPDS 88-1007) [40-42].

The average crystallite size of the synthesized ZrO_2 was computed by using Debye- Scherer formula [40].

$$D_{hkl} = 0.89\lambda / (\beta \mathrm{Cos}\theta) \quad (4)$$

Where K = 0.9 is the shape factor, D_{hkl} - is the crystallite size along with (h k l) direction, λ is the wavelength for the kα component employed in XRD (Cu radiation: 1.5406), β (FWHM) of the diffraction peak, θ -is a Bragg's angle. The average crystallite size of the ZrO_2 (600ºC) nanoparticles was observed to be 4.2 nm respectively.

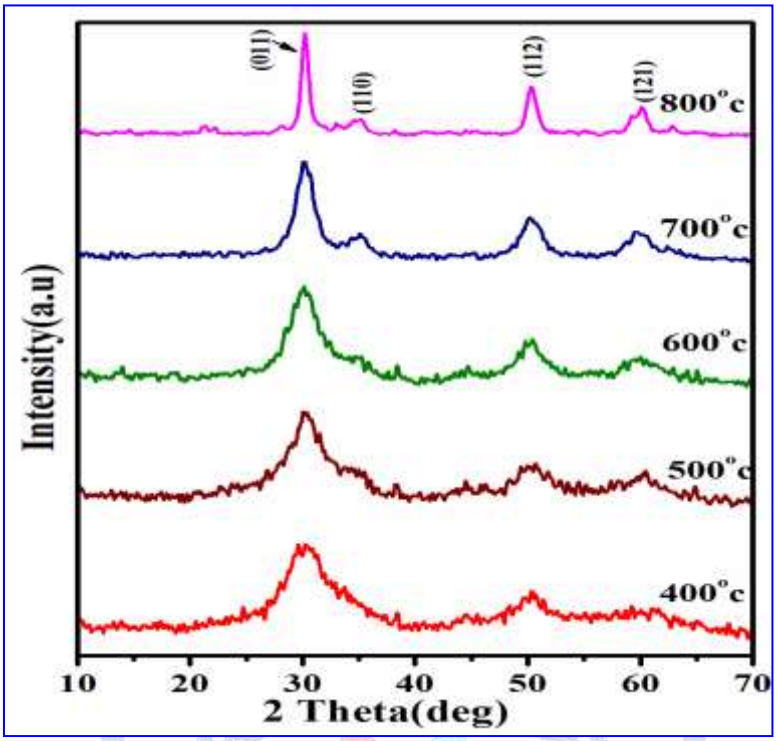

Figure 2. XRD patterns of nanosized precursor ZrO_2 calcined at different temperatures

Table 1. Materials and temperature, crystallite size, phase and band gap of pure ZrO_2 (400, 500, 600, 700 and 800 °C) NPs

Samples No	Materials Temperatures (°C)	Crystallite size (nm)	Phases	Band gap (E_g)
1	ZrO_2 (400°C)	2.6	Tetragonal (t)	5.16 eV
2	ZrO_2 (500°C)	2.0	Tetragonal (t)	5.34 eV
3	ZrO_2 (600°C)	2.9	Tetragonal (t)	5.12 eV
4	ZrO_2 (700°C)	3.8	Tetragonal (t)	5.27 eV
5	ZrO_2 (800°C)	10.2	Tetragonal (t)	5.20 eV

3.3. FT- IR analysis

The FT-IR spectra of ZrO_2 samples were analyzed in the range of 4000–400 cm^{-1}. In order to identify the chemical bonding pertaining to the synthesized ZrO_2 samples. Derived samples calcined at 400, 500, 600, 700 and 800 °C are enlarged in Fig.3. The spectrum exhibit peaks are located at 451, 509, 648, 808, 961, 1300, 1425, 1571, 2937, 2978 and 3411cm^{-1}. The peaks at 1,571 and 3,411 cm^{-1} are ascribed to the bending ν(O–H) and stretching δ(OH) vibrations of O–H (hydroxyl bond) due to absorbed of H_2O and alcohol molecules occluded into the samples [25][39][43][44]. In addition, information two hydroxyl groups were found in the XPS of species (O1S and O2S) in ZrO_2 was reliable with FTIR spectrum. Very weak vibrations at 2937 and 2978 cm^{-1}, by reason of the C–H bonds arising from the carbon chain were adsorbed of the surface molecules associated with in metal (ZrO_2) [45].

The pointed peak at 1571 cm^{-1} and 1425 is attributed to the stretching modes of vibrations in asymmetric and symmetric C=O bonds are observed. Furthermore, the weak absorption peak at 1300 cm^{-1} is due to the O–H stretching of the absorbed H_2O re-absorption through the storage of the sample in ambient air [37][46]. The absorption peak at 808 cm^{-1} originated from bending modes of vibration in Zr-O compound [8]. The strong and representative, broad band observed at 451–648 cm^{-1} is attributed to the Zr–O –Zr and Zr–OH vibrations bond stretching and bending modes of the metal, respectively [39][46][47]. From additional no reduction of H_2O, acetate anions and hydroxyl groups on the product showed no noticeable changes in peak position.

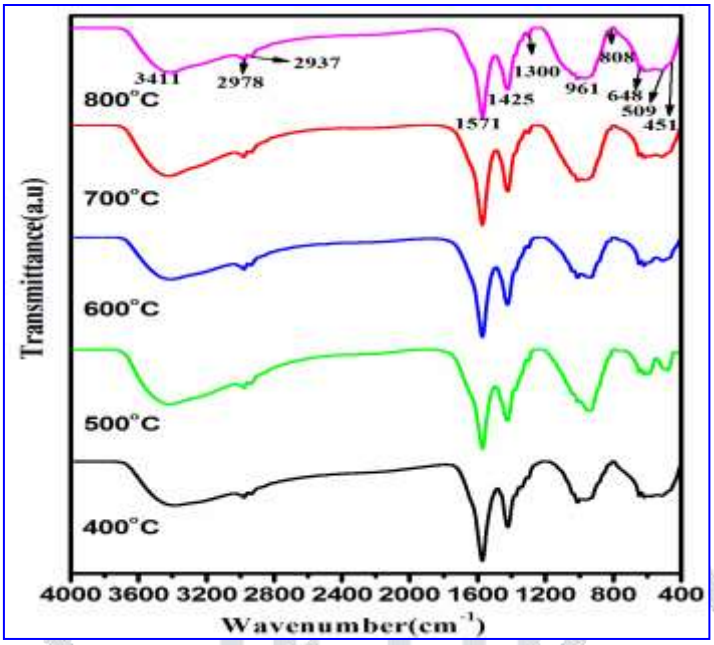

Figure 3. FT-IR spectra of ZrO_2 Nanoparticles calcined at different temperatures

3.4. Ultraviolet-visible–diffuse reflectance spectroscopy (UV-DRS)

The band gap of the synthesized ZrO_2 samples was received from the UV- DRS spectra. The UV–Vis diffuse reflectance spectrum of ZrO_2 calcined at varying temperature are shown in Fig.4, respectively. All these products exhibit good optical quality in the UV region, since DRS spectrum, show complete reflectance in the 204- 400 nm (5.1-5.34 eV) range, metals due to the O^{2-} to Zr^{4+} charge-transfer transition. An additional peak strongly is observed at 379 nm the positions indicated a blue shifted. It gives formation of a mid-band state by N2p orbital within Eg may be dependable for the extra peak. In addition, oxygen defect band states could also be created [48-50].

As the increasing temperature, the peak intensity decreased with increase in the reflectance spectrum is taking place due to quantum confinement effect [51]. The reason of obtaining optical band gap values for ZrO_2 NPs was used well-known equation given by (5)

$$\alpha = \frac{A(h\nu - E_g)^{1/2}}{h\nu} \quad (5)$$

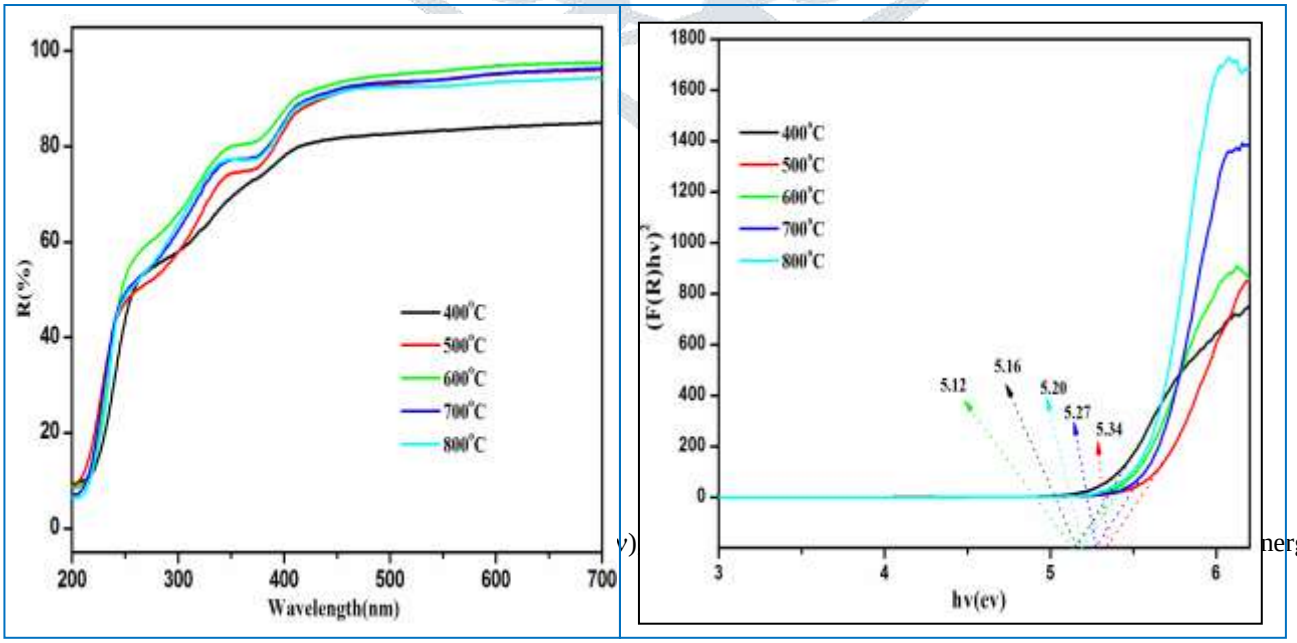

v) nergy

Figure 4. a) UV–DRS spectra of ZrO_2 nanoparticles calcined at different temperatures
b) Plot of band gap energy for ZrO_2 nanoparticles annealed at different temperatures

(hv) respectively. By plotting shows of $(\alpha h\nu)^2$ versus $h\nu$ to photon energy measured band gap (Eg) (5.1-5.34 eV) respectively, Table.1.can be noticed clearly, when calcined from 400 to 800 ^oC as corresponding to increase with decreased optical band gaps (5.16, 5.34, 5.12, 5.27, and 5.20 eV) respectively. In the present study, the intensity of the peaks increasing slightly decreasing compared to 600^oC (5.12 eV). The highest 5.34 eV band gap (Eg) occurred in 500 ^oC when comparing to that 400, 600, 700, 800 ^oC of the samples. ZrO_2 samples exhibited by different Eg mainly depended on synthesis condition, thermal effect [31].

3.5. Morphological study

The FESEM micrographs of ZrO_2 sample calcined at 600 ^oC with different magnification images are shown in fig 5a and 5b. From the photographs, it can be clearly observed that the ZrO_2 nanoparticles exhibit irregular and less uniform spherical morphology with high agglomeration was obtained as well as size could not be finely resolute from micrograph [40, 52].

Further, ZrO_2 nanoparticles were analyzed to the EDX spectrum presented in Fig. 5c. The signal confirmed the characteristic of zirconium (Zr) and oxygen (O) species from the ZrO_2 sample. From the EDX spectrum, all the peaks of Zr and O are allotted without any signals unidentified, it's proving the formation of ZrO_2 (Zirconium oxide) and purity clearly indicated that the synthesized products.

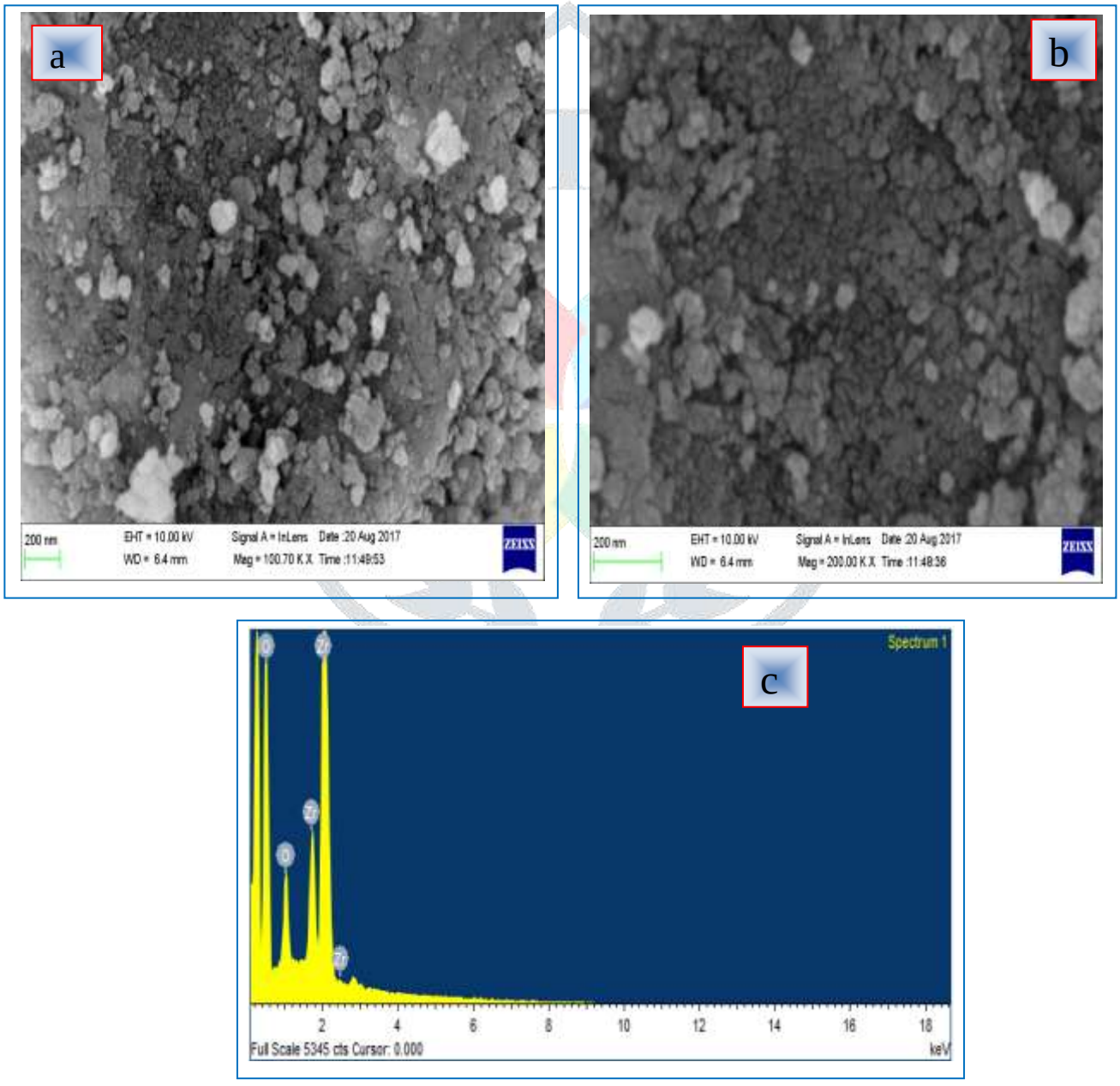

Figure 5. FESEM images of ZrO_2 nanoparticles calcined at 600^oC optimum level ions (a, b) different magnification images and corresponding EDX patterns (c)

3.6. Photocatalytic activity

The photocatalytic activity of synthesized ZrO_2 (600ºC) nanoparticles was evaluated by using degradation of MV and MB solution, under UV light irradiation. Prior to irradiation, the UV- visible absorption of Methyl violet and Methyl blue dyes have a weak and a strong peak at 291 and 596 nm, 312 and 599 nm respectively. It can be seen in Fig. 6a. 6b. After adding ZrO_2 (600ºC) catalyst into MV and MB solution, the photodegradation of MV and MB dyes increases for various time intervals. Figure 6a & 6b displays the absorption spectra of MV and MB dye solution at various irradiation times in the presence of ZrO_2 (600ºC) catalyst. Once the irradiation was started, the weak and strong absorption intensity peaks of MV and MB dyes solution gradually decreased with increases time intervals. The decrease in the absorbance peak intensity indicates the photodegradation of the MV and MB dye solution with passes of time and slightly gradually vanished after 70 min. This ZrO_2 (600ºC) product shows good photocatalytic activity in both dyes (MV and MB). The possible reason is a lesser crystalline size and larger surface area. Fig.7 shows the degradation percentage (%) of MV and MB dyes at various time intervals, it can be computed by the following expression:

$$\text{The Degradation \%} = \frac{C_0 - C_t}{C_0} \times 100\%$$

$$= \frac{A_0 - A_t}{A_0} \times 100\% \qquad (6)$$

Where C_O is the initial concentration of MV and MB dyes, C_t is the residual concentration of MV and MB dye after irradiation time intervals (0-60 min), A_t is the intensity of the absorbance peak after any irradiated time t and A_o is the intensity of the absorbance peak at time t =0.

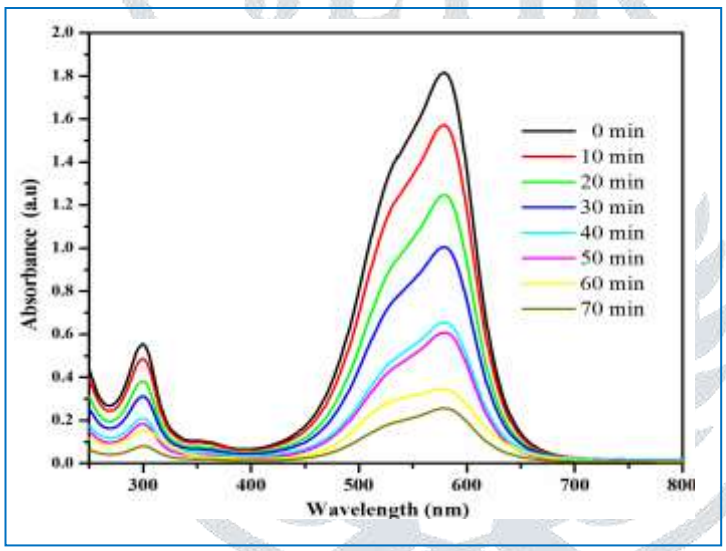

Fig. 6a Time dependent UV–Vis absorption spectra of the photocatalytic degradation of MV in the presence of ZrO_2 (600ºC) nanoparticles.

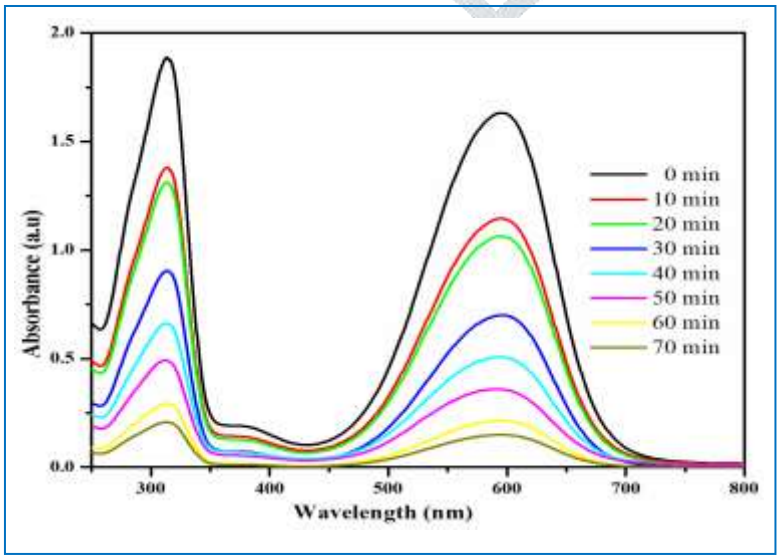

Fig. 6b. Time dependent UV–Vis absorption spectra of the photocatalytic degradation of MB in the presence of ZrO_2 (600ºC) nanoparticles.

The value of C/Co is computed for all the aqueous solution (neat MV, MB dyes, the solution of MV dye with ZrO_2 (600ºC) and solution of MB dye with ZrO_2 (600ºC). When the aqueous solution of MV and MB dyes are UV irradiated for 70 min, the degradation of MV and MB dyes is found to be <7% and <9%. When ZrO_2 (600ºC) catalyst is inserted to the Methyl violet and Methyl blue dyes solution, the photodegradation of Methyl violet and Methyl blue dyes solution dramatically increases up to 82 % and 88% for 70 min of irradiation intervals. Both dyes (MV and MB) solution shows the outstanding photocatalytic activity of ZrO_2 (600ºC).

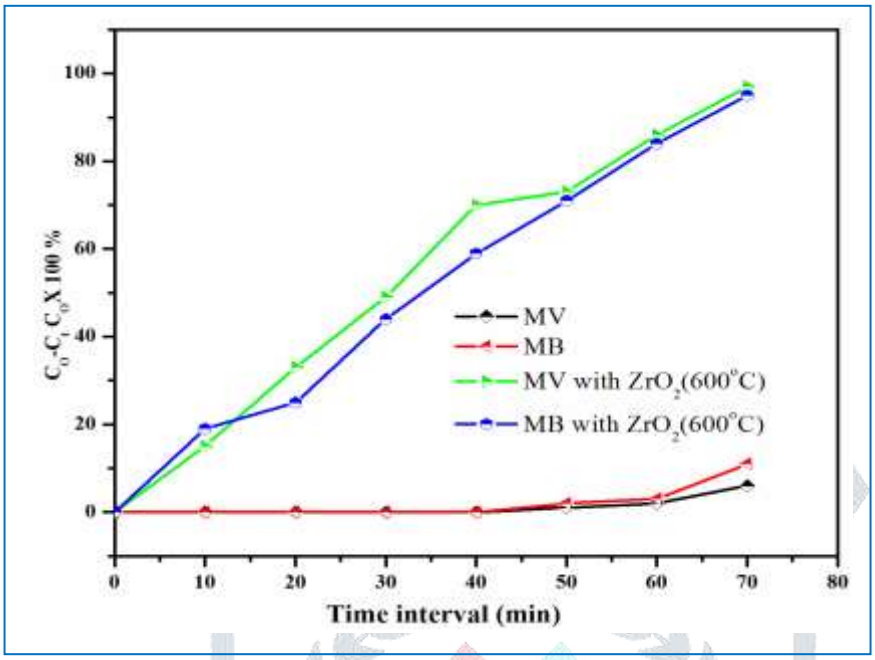

Fig. 7. Plot of (C/C0) versus time for the photodegradation of MV and MB dyes, MV with ZrO_2 (600ºC) and MB with ZrO_2 (600ºC) sample under UV irradiation

3.7. Photocatalytic degradation mechanism

The photocatalytic degradation mechanism of MV and MB dyes of ZrO_2 (600ºC) catalysts is shown in Fig.8. The overall photodegradation process can be described in the following ways. When a ZrO_2 (600ºC) nanoparticles is irradiated under the Ultra Violet (UV) light, the generated electrons will quantum jump from valence band (VB) to the conduction band (CB), that creates some holes in the valence band (equation 7). The generated holes in the valence band of ZrO_2 react with hydroxyl anion to produce hydroxyl radicals (·OH) is the denoted equation 8. The generated holes are permitted to dissociation of H2O molecules in the dye (MV and MB) solution, creating radicals (Equation 9). To more, the generated electron in the conduction band of ZrO_2 may interact with O_2 molecules to produce superoxide anions ($\cdot O_2^-$) radicals (equation 10). Finally, the created radicals such as hydroxyl anion and superoxide anion interact with the dyes (MV and MB) solution to degraded, it completely is denoted equation 11 and 12. The potential reactions reporting the above-discussed matter are given following ways [6, 53].

$ZrO_2 + h\nu \rightarrow e^-(CB) + h^+ (VB)$ (7)

$O_2 + e^- \rightarrow \cdot O_2^-$ (8)

$h^+ + OH^- \rightarrow \cdot OH$ (9)

$h^+ + H_2O \rightarrow H^+ + \cdot OH^-$ (10)

$\cdot OH^-$ + Methyl violet and Methyl blue → Degradation products (11)

$\cdot O_2^-$ + Methyl violet and Methyl blue → Degradation products (12)

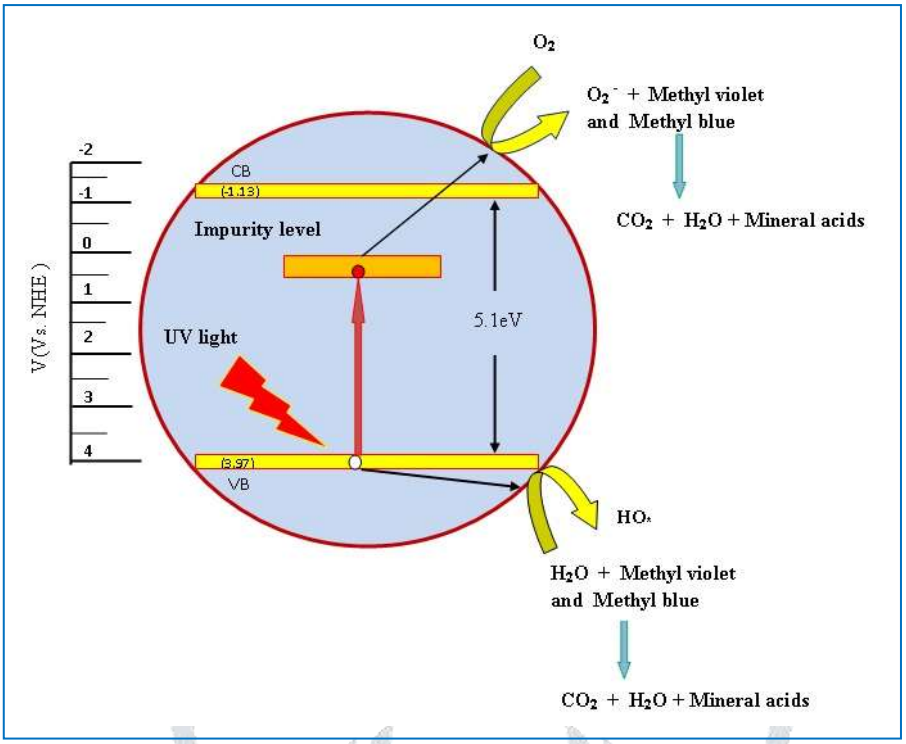

Figure 8. Proposed mechanism for the photocatalytic degradation of MV and MB dyes over ZrO_2 (600ºC) Photocatalysts.

4.Conclusion

In this connection, ZrO_2 nanoparticles calcined at 400, 500, 600, 700, and 800 ºC have been prepared successfully precipitation process using relevant precursor materials. The thermal analysis of the as-prepared product exhibited various transitions (endothermic and exothermic) and thermal stability. From the TG-DTA results revealed that 400ºC could be the optimum level of annealing for the harvest of the pure phase of ZrO_2, However, crystalline improvement arrived after a high degree of annealing. The XRD analysis proposed the formation of t-ZrO_2 phase, with no phase different from 400 to 800ºC, which indicated increasing crystallinity. The average crystallites size of 4.5 nm. From UV– DRS results could be found that the band gap 5.1eV (600ºC) comparison to other high band gaps with increasing calcination temperatures. The ZrO_2 (600ºC) nanoparticles demonstrated the good photocatalytic activity toward the photodegradation of Methyl violet and Methyl blue dyes.

5. Acknowledgments

We also thank Dr. SP. Meenakshisundaram, Former chairman, Principle investigator DST- SERB, Department of Chemistry, Annamalai University, for recording UV-DRS. The authors wish to thank Dr. V. Ramaswamy, Professor, and Head, Department of Physics, Annamalai University, for providing necessary facilities to carry out this work.

References

[1] S. N. Basahel, T. T. Ali, M. Mokhtar, and K. Narasimharao, "Influence of crystal structure of nanosized ZrO_2 on photocatalytic degradation of methyl orange," *Nanoscale Res. Lett.*, 10.73,1–13, 2015.

[2] D. Gümü and F. Akbal, "Photocatalytic Degradation of Textile Dye and Wastewater," *Water Air Soil Pollut*, 216, 117–124, 2011.

[3] M. F. Abid, A. A. Abdulrahman, and N. H. Hamza, "Hydrodynamic and kinetic study of a hybrid detoxification process with zero liquid discharge system in an industrial wastewater treatment," *J. Environ. Heal. Sci. Eng.*, 12:145,1–17, 2014.

[4] S. Ong, O. Min, and L. Ho, "Solar photocatalytic degradation of mono azo methyl orange and diazo reactive green 19 in single and binary dye solutions : adsorbability vs photodegradation rate," *Env. Sci Pollut Res*, 20, 3405–3413, 2013.

[5] S. Polisetti, P. A. Deshpande, and G. Madras, "Photocatalytic Activity of Combustion Synthesized ZrO_2 and ZrO_2 À TiO_2 Mixed Oxides," |*Ind. Eng. Chem. Res*, 50, 12915–12924, 2011.

[6] S. Kumar and A. K. Ojha, "Oxygen vacancy induced photoluminescence properties and enhanced photocatalytic activity of ferromagnetic ZrO_2 nanostructures on methylene blue dye under ultra-violet radiation," *J. Alloys Compd.*, 644, 654–662, 2015.

[7] H. F. RAGaneev, MBaba, MMorita, DRau, "Nonlinear optical properties of CdS and ZnS nanoparticles doped into zirconium," *J. Opt. A Pure Appl. Opt.*, 6, 447–453, 2004.

[8] V. A. Online, Z. Shu, X. Jiao, and D. Chen, "Hydrothermal synthesis and selective photocatalytic properties of tetragonal star-like ZrO_2 nanostructures 3," *CrystEngComm*, 2013.

[9] S. Chang and R. Doong, "The Effect of Chemical States of Dopants on the Microstructures and Band Gaps of Metal-Doped ZrO_2 Thin Films at Different Temperatures," *J. Phys. Chem*, 108, 18098–18103, 2004.
[10] J. Wang, W. Yin, X. He, Q. Wang, M. Guo, and S. Chen, "Good Biocompatibility and Sintering Properties of Zirconia Nanoparticles Synthesized via Vapor-phase Hydrolysis," *Nat. Publ. Gr.*, 6, 1–10, 2016.
[11] K. Smits, D. Olsteins, A. Zolotarjovs, K. Laganovska, and D. Millers, "Doped zirconia phase and luminescence dependence on the nature of charge compensation," *Nat. Publ. Gr.*, 7, 1–8, 2017.
[12] H. Mudila, S. Rana, and M. G. H. Zaidi, "Electrochemical performance of zirconia / graphene oxide nanocomposites cathode designed for high power density supercapacitor," *J. Anal. Sci. Technol.*, 7, 1–11, 2016.
[13] J. D. Fidelus and A. Karbowski, "Positron-Annihilation , Structural and Optical Studies on Properties of Nanostructured ZrO_2, ZnO, Bi_2O_3 and ZnO Bi_2O_3," *ACTA Phys. Pol. A*, 120, 66–68, 2011.
[14] C. A.-A. F Ramos-Brito MGarc´ ıa-Hip´ olito and O. A.-F. and C. Falcony, "Characterization of luminescent praseodymium-doped ZrO_2 coatings deposited by ultrasonic spray pyrolysis," *J. Phys. D. Appl. Phys.*, 40, 6718–6724, 2007.
[15] N. Korsunska, M. Baran, and I. Vorona, "Impurity-Governed Modification of Optical and Structural Properties of ZrO_2 -Based Composites Doped with Cu and Y," *Nanoscale Res. Lett.*, 12:157, 1–11, 2017.
[16] C. Mcmanamon, J. D. Holmes, and M. A. Morris, "Improved photocatalytic degradation rates of phenol achieved using novel porous ZrO_2 -doped TiO_2 nanoparticulate powders," *J. Hazard. Mater.*,193,120–127, 2011.
[17] N. S. S. S. K. Dinakaran, "Synthesis , structural and optical characterization of ZrO_2 core–ZnO@SiO_2 shell nanoparticles prepared using co-precipitation method for opto-electronic applications," *J Mater Sci Mater Electron*, 25, 5078–5083, 2014.
[18] S. Basu, S Varma *et al.*, "X-ray absorption spectroscopy of doped ZrO_2 systems X-ray absorption spectroscopy of doped ZrO_2 systems," *J. Appl. Phys. 111*,111, 1–9, 2012.
[19] K. Utt, S. Lange, M. Järvekülg, H. Mändar, P. Kanarjov, and I. Sildos, "Structure and optical properties of Sm-doped ZrO_2 microrolls," *Opt. Mater. (Amst).*, 32, 823–826, 2010.
[20] F. Zhang, P. J. Chupas, S. Lun, and Lui, "In situ Study of the Crystallization from Amorphous to Cubic Zirconium Oxide : Rietveld and Reverse Monte Carlo Analyses," *Chem. Mater.*,19, 3118–3126, 2007.
[21] W. Han, B. Ding, M. Park, F. Cui, S. Chae, and H. Kim, "Insight into the precursor nanofibers on the flexibility of La_2O_3 -ZrO_2 nanofibrous membranes," *DE GRUYTER*, 17, 243–248, 2017.
[22] K. V. A. Kumar, R. Amanchi, B. Sreedhar, and P. Ghosal, "Phenol and Cr (VI) degradation with Mn ion doped ZnO under visible light photocatalysis," *RSC Adv.*, 7, 43030–43039, 2017.
[23] L. Y. Zhu, X. Q. Wang, G. H. Zhang, Q. Ren, and D. Xu, "Structural characterization and photocatalytic activity of B_2O_3/ZrO_2–TiO_2 mesoporous fibers," *Appl. Catal. B Environ.*,103, 428–435, 2011.
[24] H. Xie, J. Lu, and Shekhar, "Synthesis of Na-Stabilized Nonporous t-ZrO_2 Supports and Pt/t-ZrO_2 Catalysts and Application to Water-Gas-Shift Reaction," *ACS Catal.*, 3, 61–73, 2013.
[25] C. Lin, C. Zhang, and J. Lin, "Phase Transformation and Photoluminescence Properties of Nanocrystalline ZrO_2 Powders Prepared via the Pechini-type Sol - Gel Process," *J. Phys. Chem. C*,111, 3300–3307, 2007.
[26] M. A. Corte, P. Ingenieri, and J. A. Wang, "Influence of Synthesis Methods on Tungsten Dispersion , Structural Deformation , and Surface Acidity in Binary WO_3 - ZrO_2 System," *J. Phys. Chem. B*, 109, 22730–22739, 2005.
[27] L. Li, L. Wang, and W. Zhang, "Urchin-like CdS/ZrO_2 nanocomposite prepared by microwave-assisted hydrothermal combined with ion-exchange and its multimode photocatalytic activity," *J Nanopart Res*, 16, 1–14, 2014.
[28] H. Chen, J. Shi, W. Zhang, and M. Ruan, "Incorporation of Titanium into the Inorganic Wall of Ordered Porous Zirconium Oxide via Direct Synthesis," *Chem. Mater.*, 13, 1035–1040, 2001.
[29] M. Garc and E. Mart, "Preparation and characterization of photoluminescent praseodymium-doped ZrO_2 nanostructured powders," *J. Phys. D. Appl. Phys.*, 37, L13–L16, 2004.
[30] S. K. Durrani, M. Rehman, Arif, and B. Mohammad, "The impact of sintering promoter oxides on magnesia-doped zirconia crystals synthesized by sol spray pyrolysis process," *Nucl.*, 48, 91–99, 2011.
[31] S. Kumar, S. Bhunia, and A. K. Ojha, "Effect of calcination temperature on phase transformation , structural and optical properties of sol – gel derived ZrO_2 nanostructures," *Phys. E J.*, 66, 74–80, 2015.
[32] J. Rochford, E. Galoppini, R. U. V, and W. Street, "Zinc (II) Tetraarylporphyrins Anchored to TiO_2, ZnO, and ZrO_2 Nanoparticle Films through Rigid-Rod Linkers," *Langmuir*, 24, 5366–5374, 2008.
[33] Y. Wang, W. Gao, and H. Wang, "Morphology and activity relationships of macroporous CuO–ZnO – ZrO_2 catalysts for methanol synthesis from CO_2 hydrogenation," *Rare Met.*, 35, 790–796, 2016.
[34] J. Wang, J. Huang, J. Meng, Q. Li, and J. Yang, "Double-hole codoped huge-gap semiconductor ZrO_2 for visible-light photocatalysis," *Phys. Chem. Chem. Phys.*, 18, 17517–17524, 2016.
[35] H. Wang, G. Li, Y. Xue, and L. Li, "Hydrated surface structure and its impacts on the stabilization of t -ZrO_2," *J. Solid State Chem. 180*, 2790–2797, 2007.
[36] S. G. Botta, J. A. Nav, C. Hidalgo, G. M. Restrepo, and M. I. Litter, "Photocatalytic properties of ZrO_2 and Fe/ZrO_2 semiconductors prepared by a sol – gel technique," *J. Photochem. Photobiol. A Chem.*, 129, 89–99, 1999.
[37] H. Zheng, K. Liu, H. Cao, and X. Zhang, "L -Lysine-Assisted Synthesis of ZrO_2 Nanocrystals and Their Application in Photocatalysis," *J. Phys. Chem.*, 113, 18259–18263, 2009.
[38] M. Rezaei, S. M. Alavi, S. Sahebdelfar, L. Xinmei, and L. Qian, "CO_2 - CH_4 Reforming over Nickel Catalysts Supported on Mesoporous Nanocrystalline Zirconia with High Surface Area," *Energy & Fuels 2007*, 21, 581–589, 2007.

[39] C. Zhang, C. Li, and Yang, "Tunable Luminescence in Monodisperse Zirconia Spheres," *Langmuir*, 25, 7078–7083, 2009.
[40] S. Zinatloo-ajabshir and M. Salavati-niasari, "Facile route to synthesize zirconium dioxide (ZrO_2) nanostructures : Structural , optical and photocatalytic studies," *J. Mol. Liq.*, 216, 545–551, 2016.
[41] M. W. Kadi and R. M. Mohamed, "Enhanced Photocatalytic Activity of ZrO_2 -SiO_2 Nanoparticles by Platinum Doping," *Int. J. Photoenergy*, 2013, 1–7, 2013.
[42] G. J. Zhou, F. Gu, S. F. Wang, and M. K. L, "Effect of Dy 3 þ doping and calcination on the luminescence of ZrO_2 nanoparticles," *Chem. Phys. Lett.*, 380, 185–189, 2003.
[43] L. Renuka, K. S. Anantharaju, and Sharma, "Hollow microspheres Mg-doped ZrO_2 nanoparticles: Green assisted synthesis and applications in photocatalysis and photoluminescence," *J. Alloys Compd.*, 2016.
[44] S. L. Jangra, K. Stalin, and Dilbaghi, "Antimicrobial Activity of Zirconia (ZrO_2) Nanoparticles and Zirconium Complexes," *J. Nanosci. Nanotechnol.*, 12,7105–7112, 2012.
[45] M. Salavati-niasari, M. Dadkhah, and F. Davar, "Pure cubic ZrO_2 nanoparticles by thermolysis of a new precursor," *Polyhedron*, 28, 3005–3009, 2009.
[46] K. Gnanamoorthi, M. Balakrishnan, R. Mariappan, and E. R. Kumar, "Effect of Ce doping on microstructural , morphological and optical properties of ZrO_2 nanoparticles," *Mater. Sci. Semicond. Process.*, 30,518–526, 2015.
[47] I. Das and G. De, "Zirconia based superhydrophobic coatings on cotton fabrics exhibiting excellent durability for versatile use," *Nat. Publ. Gr.*, 5, 1–12, 2015.
[48] S. T. Hanggara Sudrajat , Sandhya Babel , Hiroshi Sakai, "Rapid enhanced photocatalytic degradation of dyes using novel," *J. Environ. Manage.*, 165, 224–234, 2016.
[49] K. V. R. Chary, G. V. Sagar, and C. S. Srikanth, "Characterization and Catalytic Functionalities of Copper Oxide Catalysts Supported on Zirconia," *J. Phys. Chem.*,111, 543–550, 2007.
[50] N. C. Sagaya, A. Manikandan, L. J. Kennedy, and J. J. Vijaya, "Comparative investigation of zirconium oxide (ZrO_2) nano and microstructures for structural , optical and photocatalytic properties," *J. Colloid Interface Sci.*, 389, 91–98, 2013.
[51] N. Kannadasan, N. Shanmugam, K. Sathishkumar, S. Cholan, R. Ponnguzhali, and G. Viruthagiri, "Optical behavior and sensor activity of Pb ions incorporated ZnO nanocrystals," *Spectrochim. ACTA PART A Mol. Biomol. Spectrosc.*, 1–24, 2015.
[52] C. Hang, Q. Li, S. Gao, and J. K. Shang, "As (III) and As (V) Adsorption by Hydrous Zirconium Oxide Nanoparticles Synthesized by a Hydrothermal Process Followed with Heat Treatment," *Ind. Eng. Chem. Res.*, 51,353–361, 2012.
[53] M. Jothibas, C. Manoharan, S. J. Jeyakumar, P. Praveen, I. K. Punithavathy, and J. P. Richard, "Synthesis and enhanced photocatalytic property of Ni doped ZnS nanoparticles," *Sol. Energy*, 159, 434–443, 2018.